Molecular Logic

Optically Controlled Thermochromic Switching for Multi-Input Molecular Logic

Liang Fei, Weidong Yu, Zonghuai Wu, Yunjie Yin, Kasper Moth-Poulsen,* and Chaoxia Wang*

Abstract: Leuco dye-based thermochromic materials offer enormous potential for visible molecular logic due to the appealing reversible color-changing effect. The stable color state is uncontrollable as it depends only on the spontaneous protonation of the leuco dye and color developer. There is still a challenge to propose an effective approach to control bistable color function at required temperature. A family of azobenzenes with various alkyl chains (AZO(n)) is designed for protonation competition with leuco dye. The hydrogen bond and Van der Waals forces are formed between color developer and AZO(n). The color developer can be locked to provide the proton for the leuco dye by *Z*-AZO(n), while it can be released upon *Z*-to-*E* photoisomerization. The locked state can be lasted for more than 16 hours. This optically controlled leuco dye-based system demonstrates a visible sequential logic operation with four-input signals, and provides a new type of protonation-based optical control.

Molecular logic operations for information processing and computation have become a vibrant research field since the first molecular logic AND gate with non-electrical input/output signals was reported in 1993.[1] According to the principles of binary notation and Boolean language, the

input and output signals in molecular logic are expressed as zeros and ones, leading to the realization of utility functions, such as organic molecule detection, biomedical engineering and information memory.[2] Molecules respond to various stimuli in their environment such as light, temperature, pH and chemicals.[3] Among those input signals, chemical species may cause a series of problems due to the time delay of diffusion and stimulating or resetting the input. Light and temperature as physical stimuli offer an ideal opportunity for remote control with high fatigue resistance. In the majority of molecular logic gates, the output signals depend only on the correct input combination, whereas in other systems, the sequential logic operations can also influence the output results.[4] It is attractive to have optical output that can clearly be seen by human eye, without the need for advanced spectroscopic tools.[2c,5]

Leuco dye- (LD) based thermochromic (TC) materials have been widely applied in energy storage, sensors and memories, due to their low cost, full-color reproduction and excellent durability.[5c,6] In this thermochromic process, the colors reversibly change with temperature, because of the protonation formation or destruction between the color former and color developer.[6a,7] For example, the deprotonation process of 7-anilino-3-diethylamino-6-methyl fluoran (ADMF, color former) occurs above the T_m (Figure 1a) and is supported by the bisphenol A (BPA, color developer) below the T_m. Due to the spontaneous protonation under cooling process, the color display over T_m cannot be conserved. Since the objective of our research is to augment the color changing function of the ADMF-BPA materials, we try to control this LD-based system using interactions with molecular photoswitches, molecules that isomerizes upon exposure to light. The azobenzene family is the most commonly used photoswitch, attributed to its advantages of controllably quantitative and bidirectional *E-Z* photoisomerization.[8] The change in geometry upon isomerization, allows us to tailor the molecular polarity, sterical effects and conjugation.[9] In case of photochromic lock/block, one isomer functions as a strong lock to isolate the BPA, while the converted isomer is, inert in the LD-based system. In recent endeavors of azo-based structural modification, substituting one or both side of phenyl rings is used to create photo locks.[9,10]

Herein, we have modified AZO based photoswitches with alkyl chains (AZO(n), Figure 1b) to promote the interaction between azobenzene and BPA so that it competes with the ADMF-BPA interaction. We also present a novel optically controlled LD-based system with specially
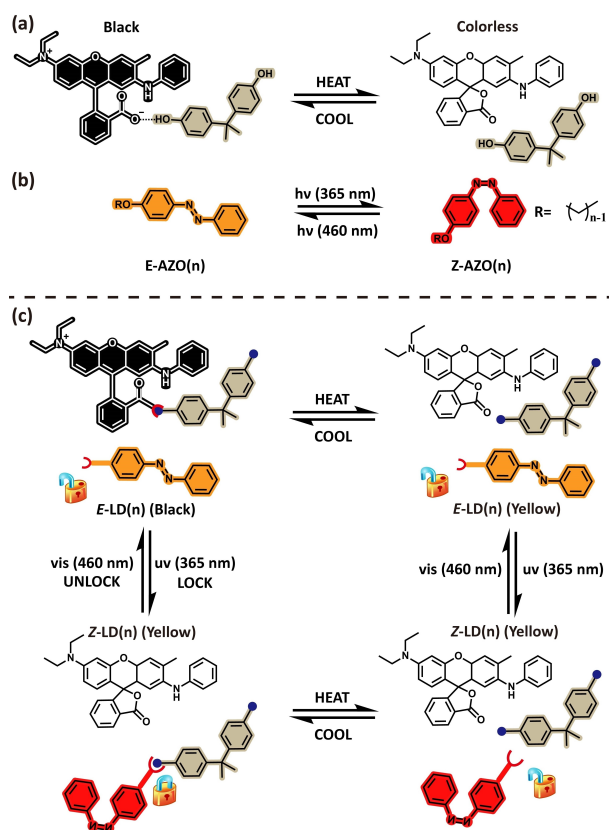
---

[*] L. Fei, W. Yu, Z. Wu, Prof. Y. Yin, Prof. C. Wang
School of Textile Science and Engineering, Jiangnan University
1800 Lihu Road, 214122, Wuxi (China)
E-mail: wangchaoxia@sohu.com

L. Fei, Prof. K. Moth-Poulsen
Department of Chemistry and Chemical Engineering, Chalmers
University of Technology
Gothenburg 41296 (Sweden)
E-mail: kasper.moth-poulsen@chalmers.se

Prof. K. Moth-Poulsen
The Institute of Materials Science of Barcelona, ICMAB-CSIC
08193, Bellaterra, Barcelona (Spain)

Prof. K. Moth-Poulsen
Catalan Institution for Research & Advanced Studies, ICREA
Pg. Lluís Companys 23, Barcelona (Spain)

Angew. Chem. **2022**, *134*, e202212483 (1 of 6)

© 2022 The Authors. Angewandte Chemie published by Wiley-VCH GmbH

Figure 1. The reversible structure changes of a) ADMF-BPA and b) AZO(n). c) The concept of thermochromic switching lock.

designed azobenzene. As detailed in Figure 1c, the color of the original state of E-LD(n) with E-AZO(n) is black. At higher temperatures (above T_m), the conjunction of ADMF is broken resulting in a blue shift of light absorption. The color change from black to yellow observed is afforded only by E-AZO(n). This is the common thermochromic phenomenon and mechanism, meaning that the E-AZO(n) negligibly impacts the ADMF protonation. We decide to irradiate E-AZO(n) with light at 365 nm (UV light), and notably the color also turns to yellow even at low temperature in the solid state. After 460 nm irradiation, the Z-LD(n) backconverts reforming the conjugation evident by color returning to black. This feature unambiguously demonstrates that Z-AZO(n) locks the BPA to break the ADMF-BPA interaction. When the BPA is locked by Z-AZO(n), ADMF presents only in ring-closed colorless state.

Concerning the photoisomerization property and compatibility of AZO(n) in optically controlled LD-based system, the highest color contrast (expressed by difference, ΔE_{cmc}) is observed for AZO(14) (Supporting Information). Thus, we design a optimized LD(n), where ADMF as color former, BPA as color developer, tetradecanol (TD) as organic solvent, and AZO(14) as lock. The similar alkyl chain between AZO(14) and TD promotes the isomerization and phase change temperature control.[11] We also identify the best molar ratio between those four components to obtain the highest ΔE_{cmc} responding to temperatures and
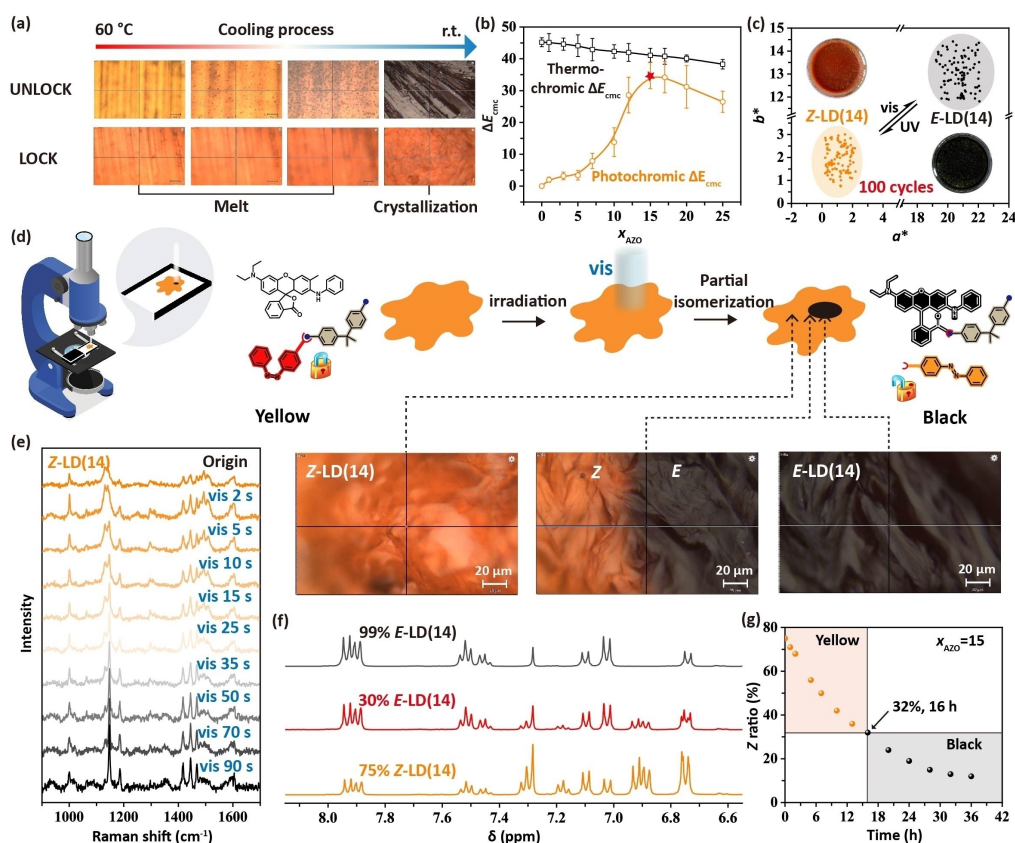
light (Figure 2b). The thermochromic and photochromic ΔE_{cmc} values change significantly at various molar fractions of AZO(14) (x_{AZO}, setting constant $x_{BPA}=3$, $x_{ADMF}=1$ and $x_{TD}=40$) with the maximum ΔE_{cmc} at a molar ratio at 15. With the increase of the x_{AZO}, the thermochromic ΔE_{cmc} decreases slightly, resulting from a deeper yellow color at high temperature but almost no change in color at lower temperature (Figure S1). At low molar AZO ratios ($x_{AZO}=$ 1–5), the color of Z-LD(14) is almost not changing, resulting in negligible photochromic effect ΔE_{cmc}. Above $x_{AZO}=10$, the E-LD(14) remains unchanged, however, the colors of Z-LD(14) are gradually lighter. The photochromic ΔE_{cmc} increases with the larger x_{AZO} but decreases mildly at the $x_{AZO}=20$. A higher AZO(14) fraction dilutes the concentration of the color developer in the system, consequently the perceived color effects.

To examine the photoisomerization lock of LD(n) in temporal and spatial control, we selectively irradiate the LD(n) in view of the Raman spectroscopy instruments in a confocal configuration. During the cooling process from 60 °C to room temperature (r.t.), the melted E-LD(14) crystallizes at 30–34 °C with color change from yellow to black (Figure 2a, Figure S2 and Movie S1). There is a precision improvement in LD(14) relative to pure LD-based system (26–36 °C), due to that the azobenzene derivatives work as a nucleator to accelerate the crystallization process. The ADMF can still protonate and deprotonate without the effect of AZO(14), so-called UNLOCK state (Table 1). The black particles appear before the complete crystallization, due to the prior crystallization of E-AZO(14) which induce a local phase change of E-LD(14). In the LOCK state, the E-LD(14) converts to the Z-LD(14) upon UV light, resulting in the no color change even at crystallization state (Figure 2a and Movie S2). The BPA preferred to combine with Z-AZO(14), rather than ring-closed ADMF. At LOCK state, the melting and crystallization features of Z-AZO(14) are absent (Figure S3), leading to no local crystallization. The π-π stacking interaction and Van der Waals' force between Z-AZO(14) molecules are disrupted because of the higher polarity and stereospecific blockade for Z-isomer.[12] The reflectance spectra show that the curve of E-LD(14) is low and almost steady in the visible region, while an obvious reflectance appears at 550–700 nm as exposed to UV light corresponding to the yellow color of Z-LD(14) (In Figure 2b). The CIE (Commission internationale de l'éclairage)

Table 1: Thermochromic switching state after applying the light input from the initial state of E-LD(14).

$I_1^{[a]}$ 365 nm light	$I_2^{[a]}$ 460 nm light	$O_1^{[b]}$ 25 °C	$O_2^{[b]}$ 60 °C	Thermochromic switching	Optical state
0	0	1	0	UNLOCK	E
1	0	0	0	LOCK	Z
0	1	1	0	UNLOCK	E
1	1	1	0	UNLOCK	E

[a] Input signals = irradiation at 365 nm and 460 nm. [b] Output signals = black color (1) and yellow color (0) at 25 °C or 60 °C.

Figure 2. a) Optical images of (UNLOCK/LOCK) *E*-/*Z*-LD(14) under cooling process from 60 °C to r.t. b) Photochromic and thermochromic color difference (ΔE_{cmc}) of LD(14) with various x_{AZO}. c) Durability upon strong lights over 100 cycles. d) Optical images of the *Z*-LD(14) that is irradiated with visible light at 25 °C and the black color state of *E*-LD(14). e) Raman spectra of LD(14) as a function of time upon visible light. f) ^{1}H NMR spectra of LD(14). g) The photo LOCK stability in a photo-LOCK state of LD(14) with $x_{AZO} = 15$ values in the dark at 25 °C. The thermal reverse conversion of LD(14) (*Z*→*E*) was monitored by ^{1}H NMR and Raman spectra (see Supporting Information).

coordinates of the LOCK and UNLOCK state are mapped in the CIE diagram (Figure S4), showing the distance in CIE coordinates between the two states.

Further refinement of the optically controlled LD-based system leads us to look into the durability even upon strong irradiation intensity and rapid temperature changes. We irradiate the LD(14) in alternate UV and visible light at our experimental conditions (of ~200 mW cm^{-2}, and 100 cycles), and the alternate temperatures are in range of 0–100 °C with heating and cooling rates of ~50 °C min^{-1}. The color parameters in L*a*b* coordinates all before and after alternating temperatures and light are only slight fluctuations (Figure 2c), which are difficult to distinguish by eyes. Those results indicate the thermochromic and photo LOCK present excellent reversibility and durability with degradation of less than 0.1 % per LOCK/UNLOCK cycle (Figure S5).

In order to investigate the photo LOCK process upon light irradiation, exposing the *Z*-LD(14) to visible light for 1.5 min triggers the *Z*-to-*E* isomerization, and the concomitant color change from yellow to black only in radiation area (Figure 2d). There is a distinct interface between different colors and negligible gradual change, indicating that the color change is occurring rapidly at narrow *Z* ratios.

We record the Raman spectra during the visible light irradiation process. The strong Raman signals with three peaks in 1475 cm^{-2}–1536 cm^{-2} disappear, which are described as the stretch vibrations of N=N and torsion of the C–N=N for *Z*-AZO(14).[13] At the left image (Figure 2d), the *Z*-LD(14) remains its LOCK state, while the right region is transferred to *E*-LD(14) (Figure S6). The intensity area of those peaks is calculated to estimate the *Z* ratios at solid state by WiRE 5.3 software (Figure S7). Very clear color change during photoisomerization is found in 35 s (Figure 2e and Movie S4), showing the BPA is unlocked from *Z*-AZO(14) and protonates the ADMF. Due to the short light irradiation time, the temperature rise from photoisomerization is minimal (less than 3 °C) (Figure S8). The accurate isomerization ratios at color change point are further estimated by ^{1}H NMR analysis (dissolved in CDCl$_3$ at 25 °C). The isomerization yields of rich *Z*- and *E*- isomers reach as high as 75 % and 99 %, respectively (Figure 2f). In case of the *Z* ratio dropping below 30 % upon visible light exposure, the color of LD(14) changes from yellow to black (called critical *Z* ratio in color change, CZC). Also, as for various x_{AZO}, the CZC increase with the decreasing of x_{AZO} (Figure S9).
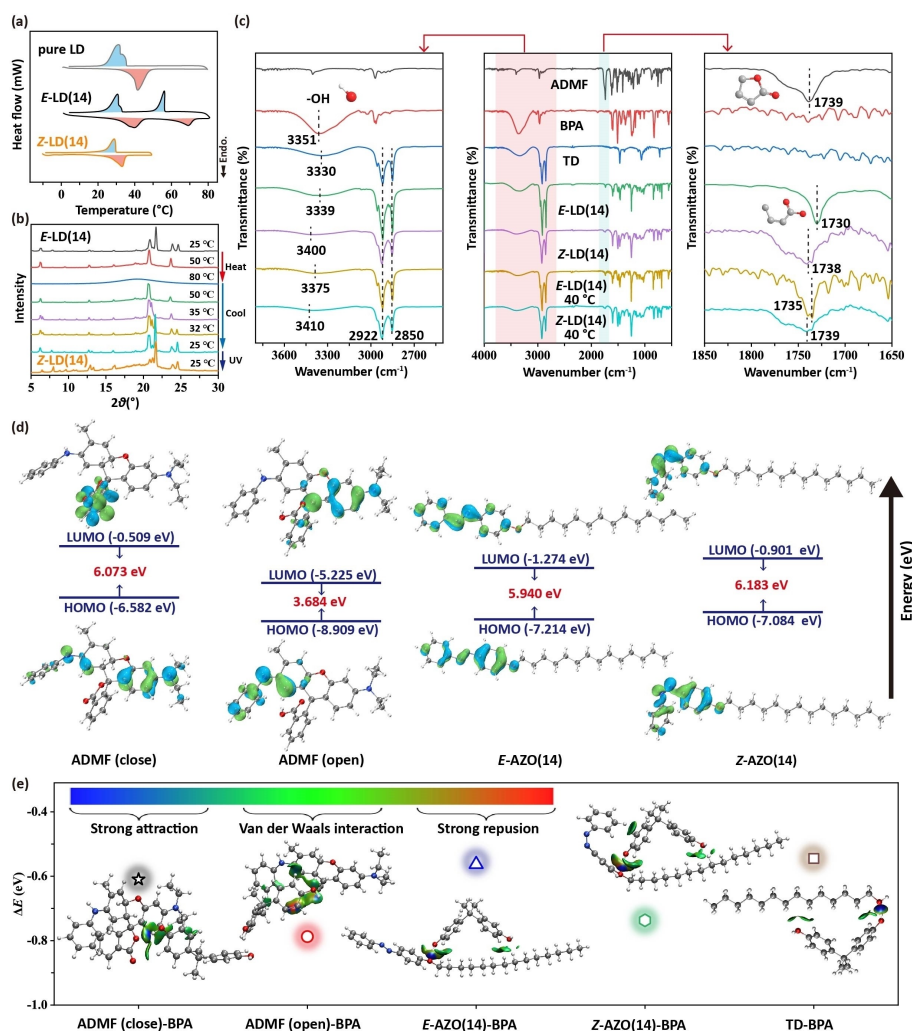
The stability of *Z*-LD(14) is measured by monitoring the color and *Z* ratio at different temperatures in the dark (Figure 2g). When the time reaches 16 h (32% *Z* ratio) at 25°C, color change is observed, which is consistent with results under visible light (Figure 2f). The longer color stable time can be achieved at lower temperature, and there is still more than 30 min to remain LOCK state at 80°C. Surprisingly, the LOCK time/life-times of *Z*-AZO(14) in LD-based system afford a ~72% increase compared to only AZO and TD (Figure S10). To conclude; the combination between BPA and *Z*-AZO(14) impedes the thermal back-conversion. It can be as a potential way to prolong half-life of metastable forms of azobenzene not only in photo LOCK state but also in solar energy storage and information memory applications.

The concept of this work is fundamentally different from that of common photochromic materials, which adjust the conjugate structures by light irradiation.[14] Instead, we present a unique approach using supramolecular chemistry and a combination of photo and thermochromic molecules to control the color change of traditional leuco dye-based thermochromic materials. The mechanisms of this type of photochromic system depend on the LD-based system (three-component thermochromic material). Therefore, three hypotheses can be considered to explain the mechanism. (1) The *Z*-AZO(n) lowers the phase change temperature in organic solvents,[11] leading to a lower thermochromic point. (2) The *Z*-AZO(n) influences the solid-solid phase formation (the crystalline *β*- or *γ*-form structures)[15] in organic solvents. (3) The *Z*-AZO(n) lock the color developer to impede leuco dye protonation.

To investigate the optically-controlled thermochromic switching mechanism, the phase change point, crystal form and molecular bonds are explored in Figure 3a–c, respectively. Figure 3a shows that the melting and crystallization points of TD are lowered in *Z*-LD(14) compared to that in *E*-LD(14) or pure LD-based system. There is a temperature gap of 5°C between LOCK and UNLOCK state, but the *Z*-LD(14) keeps yellow color even stored at 2°C (Figure S11). Thus, the hypothesis (1) is incorrect to explain the mecha-

Figure 3. a) DSC curves of pure LD and *E-/Z*-LD(14) at a rate of 5°C min⁻¹. b) in situ X-ray diffraction patterns of *E*- and *Z*-LD(14). c) FT-IR spectra of the pure components and the *E-/Z*-LD(14). d) HOMO–LUMO orbitals of ADMF and AZO(14). e) DFT-simulated blind energy and color-mapped IGM of ADMF-BPA, AZO(14)-BPA and TD-BPA.
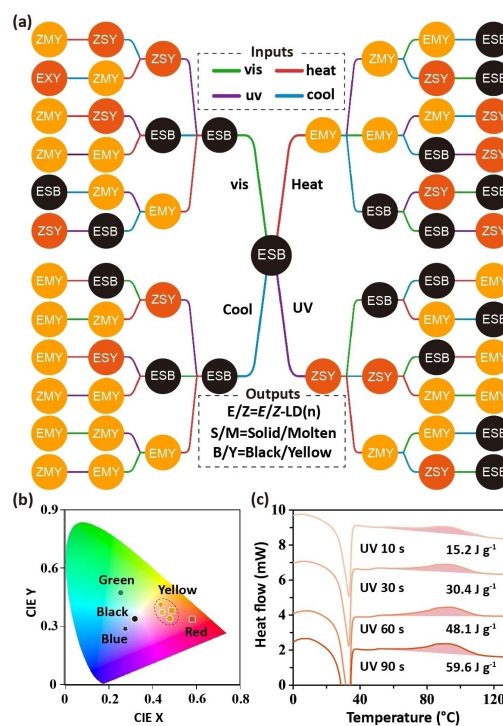
nism. There is a clear separation between the liquid-solid and solid-solid transitions in pure LD-based system and *E*-LD(14) during the cooling process (Movie S3). However, it was difficult to estimate state of *Z*-LD(14) related to the disappearance of solid-solid transition or overlap of liquid-solid and solid-solid transitions. The in situ X-ray diffraction (XRD) patterns are performed to monitor the crystal form change of the LD(14) in range of 25–80 °C at a rate of 2 °C min^{-1} (Figure 3b and Figure S12). During the heating process, the melting points of AZO(14) and TD are separated, which are also shown in DSC curve (Figure 3a). When the temperature cools to 35 °C, the liquid-solid transition of *E*-LD(14) occurs with the clear peak appearance at 21.1°. The intensity of this peak (21.1°) gradually decreases with a lower temperature, indicating the solid-solid transition formation (*β*- or *γ*-form structures). As for *Z*-LD(14), the XRD pattern of TD is similar with that in *E*-LD(14) at 25 °C, especially at $2\theta = 21.1°$. This means the liquid-solid and solid-solid transitions are overlapped, instead of only the liquid-solid transition in *Z*-LD(14). We can thus conclude that the hypothesis (2) is also incorrect.

We now turn our attention to the FT-IR spectra of the pure components and the LD(14) to identify the characteristic peak change under various temperatures and optical exposure (Figure 3c). The pure BPA and TD, the corresponding -OH stretching vibrations, are present as broad peaks at 3351 cm^{-1} and 3330 cm^{-1}, respectively. In *E*-LD(14), the mixture peak of -OH group is observed at 3339 cm^{-1} but the phenol -OH of BPA is effected by the *Z*-AZO(14) at LOCK state, shifting to the 3390 cm^{-1}. According to the peak types of hydrogen bonding between the *β*- and *γ*-forms, the –OH group peaks are single and board in all spectra of LD and *E/Z*-LD(14), meaning the formation of *β*-form.[6a,15b] In solid *E*-LD(14), the peak at 1730 cm^{-1} is ascribed to the symmetric vibration of ring opened H-bonded C=O in carboxylate group (COO^{-}). When the *E*-LD(14) is under molten state or converts to the *Z*-LD(14), the symmetric vibration of COO^{-} changes to the higher frequency of lactone carbonyl vibration (around 1738 cm^{-1}).[6a,16] We also investigated the peak shift between 1738 cm^{-1} and 1730 cm^{-1} under the super excess or none of BPA conditions to identify the ring state of ADMF, where high molar excess or none of BPA is added in LD(14) (Figure S13). All these phenomena indicate the *Z*-AZO(14) can lock the BPA to block up the protonation of ADMF.

In order to further reveal the relationship between BPA and neighboring molecules, a density functional theory (DFT) study is carried out for ADMF, AZO(14), BPA and TD. The optimized geometries of the molecules and the frontier molecular orbitals are presented in Figure 3d and Figure S14. The HOMO→LUMO transition energy of closed ADMF is higher than that of opened ADMF, showing the protonated later one is more delocalized. Compared to the *Z*-AZO(14), the HOMO→LUMO gap (corresponded to π-π* absorption band) of *E*-isomer is lower. This indicates a bathochromic shift of maximum absorption wavelength (λ_m), which is consistent with the results in UV/Vis spectra (Figure S15). The independent gradient model (IGM) maps are displayed to understand the interaction force between molecules (Figure 3e and Figure S16). The color-mapped IGM interface between BPA and

opened-ADMF presents a blue-green color, indicating strong H-bond attraction of ADMF(open)-BPA. We also explore the binding energy (ΔE) between BPA and neighboring molecules, and find that the interaction of *Z*-AZO(14)-BPA is higher than that of *E*-AZO(14)-BPA. This explains the interaction between *Z*-AZO(14) and BPA in the LD(14). The ΔE of AMDF(opened)-BPA is significantly higher than ΔE of *E*-AZO(14)-BPA, leading to the common thermochromic feature working under UNLOCK state (Figure 3e). As for *Z*-AZO(14), it is a slightly lower ΔE relative to that of AMDF-(opened)-BPA, while the doping level of *Z*-AZO(14) is higher than that of ADMF (Table S1). Therefore, the BPA can be locked by *Z*-AZO(14) and the ADMF maintains the lactone carbonyl structure.

The goal of this study is to investigate a unique approach to the photo LOCK property and to identify an optimized structure design of LD(n). For potential molecular logic applications, we envision the four-input sequences, including UV light, visible light, heating and cooling. The initial state ESB is prepared, representing the *E*-LD(14) (E) at solid state (S) with black color (B). All of the input sequences are performed, resulting in the four forms of output signals (Figure 4a). This system also can be used as a three-input sequential logic operation. For example, a specific sequence of inputs (UV-heat-cool) from ESB can induce a unique output (ESB). We also demonstrate a set-reset (S–R) latch that integrates two cross-coupled NOR gates (Figure S17). Additionally, according to the same protonation mechanism of

Figure 4. a) Predicted outputs after applying the four-input sequences from the initial state of ESB. b) CIE diagram of full color RGB system (those outputs of E/S, S/M and B/Y present the *E/Z*-LD(n), Solid/Molten state and Black/Yellow color, respectively). c) DSC results of *Z*-LD(14) charged by UV light for different time, measured at 5 °C min^{-1}.

other leuco dyes, we obtain a full RGB photo system (Figure 4b). The different colors (green, red, blue and black) can be locked upon UV light and transfer to the yellow color. During the LOCK→UNLOCK process, the LD(n) can also release the energy as a form of heat by the metastable isomer of *Z*-AZO(n) converting to the stable isomer.[12] For *Z*-LD(14), the maximum energy release reaches ~59.6 J g^{-1} (Figure 4c).

To conclude, we have demonstrated a novel approach to optically control the leuco dye thermochromic system by the use of tailored azobenzene molecular photoswitches. This strategy can add functionality to protonation-based thermochromic materials by applying designed photoswitches that can lock the relative color developer (BPA) to block the protonation of color former (ADMF) effectively. Under the LOCK state, the BPA interact with the *Z*-AZO(14), leading to a lactone carbonyl structure (colorless) of ADMF. After *Z*-AZO(14) converts to the *E*-isomer, this LOCK state can be opened, where the BPA provide the proton to the ADMF (black). This proof of concept provides an example of full-color reproduction and it is potential for information memory, keypad locks and energy storage.

Conflict of Interest

The authors declare no conflict of interest.

Data Availability Statement

The data that support the findings of this study are available from the corresponding author upon reasonable request.

[1] P. A. de Silva, N. H. Q. Gunaratne, C. P. McCoy, *Nature* **1993**, *364*, 42.

[2] a) C. Feng, T. Chen, D. Mao, F. Zhang, B. Tian, X. Zhu, *ACS Sens.* **2020**, *5*, 3116; b) J. Chen, J. Pan, C. Liu, *Anal. Chem.* **2020**, *92*, 6173; c) A. Nirmala, I. Mukkatt, S. Shankar, A. Ajayaghosh, *Angew. Chem. Int. Ed.* **2021**, *60*, 455; *Angew. Chem.* **2021**, *133*, 459; d) U. Pischel, *Angew. Chem. Int. Ed.*

[2010], *49*, 1356; *Angew. Chem.* **2010**, *122*, 1396; e) Y. Lyu, C. Wu, C. Heinke, D. Han, R. Cai, I. T. Teng, Y. Liu, H. Liu, X. Zhang, Q. Liu, W. Tan, *J. Am. Chem. Soc.* **2018**, *140*, 6912; f) R. Lopez, R. Wang, G. Seelig, *Nat. Chem.* **2018**, *10*, 746; g) J. Andréasson, D. Gust, *Photonically Switched Molecular Logic Devices*, Wiley-VCH, Weinheim, **2012**, pp. 53–78.

[3] a) S. Erbas-Cakmak, S. Kolemen, A. C. Sedgwick, T. Gunnlaugsson, T. D. James, J. Yoon, E. U. Akkaya, *Chem. Soc. Rev.* **2018**, *47*, 2228; b) S. R. Yang, J. D. Harris, A. Lambai, L. L. Jeliazkov, G. Mohanty, H. Zeng, A. Priimagi, I. Aprahamian, *J. Am. Chem. Soc.* **2021**, *143*, 16348.

[4] a) J. Andréasson, U. Pischel, *Chem. Soc. Rev.* **2018**, *47*, 2266; b) A. Dreos, Z. Wang, B. E. Tebikachew, K. Moth-Poulsen, J. Andréasson, *J. Phys. Chem. Lett.* **2018**, *9*, 6174; c) D. Margulies, C. E. Felder, G. Melman, A. Shanzer, *J. Am. Chem. Soc.* **2007**, *129*, 347.

[5] a) P. Remón, M. Hammarson, S. Li, A. Kahnt, U. Pischel, J. Andréasson, *Chem. Eur. J.* **2011**, *17*, 6492; b) L. A. Tatum, J. T. Foy, I. Aprahamian, *J. Am. Chem. Soc.* **2014**, *136*, 17438; c) G. Qian, Z. Y. Wang, *Adv. Mater.* **2012**, *24*, 1582.

[6] a) O. Panák, M. Držková, M. Kaplanová, U. Novak, M. Klanjšek Gunde, *Dyes Pigm.* **2017**, *136*, 382; b) W. Zhang, C. Wang, K. Chen, Y. Yin, *Small* **2019**, *15*, 1903750.

[7] K. Bašnec, L. S. Perše, B. Šumiga, M. Huskić, A. Meden, A. Hladnik, B. B. Podgornik, M. K. Gunde, *Sci. Rep.* **2018**, *8*, 5511.

[8] a) Y. He, Z. Shangguan, Z. Zhang, M. Xie, C. Yu, T. Li, *Angew. Chem. Int. Ed.* **2021**, *60*, 16539; *Angew. Chem.* **2021**, *133*, 16675; b) Z. Wang, R. Losantos, D. Sampedro, M.-a. Morikawa, K. Borjesson, N. Kimizuka, K. Moth-Poulsen, *J. Mater. Chem. A* **2019**, *7*, 15042; c) H. M. D. Bandara, S. C. Burdette, *Chem. Soc. Rev.* **2012**, *41*, 1809.

[9] a) M. Volgraf, P. Gorostiza, S. Szobota, M. R. Helix, E. Y. Isacoff, D. Trauner, *J. Am. Chem. Soc.* **2007**, *129*, 260; b) Y. Kim, J. A. Phillips, H. Liu, H. Kang, W. Tan, *Proc. Natl. Acad. Sci. USA* **2009**, *106*, 6489.

[10] a) M. Yamamura, Y. Okazaki, T. Nabeshima, *Chem. Commun.* **2012**, *48*, 5724; b) E. Bartels, N. H. Wassermann, B. F. Erlanger, *Proc. Natl. Acad. Sci. USA* **1971**, *68*, 1820.

[11] a) G. G. D. Han, J. H. Deru, E. N. Cho, J. C. Grossman, *Chem. Commun.* **2018**, *54*, 10722; b) G. G. D. Han, H. Li, J. C. Grossman, *Nat. Commun.* **2017**, *8*, 1446; c) L. Fei, Y. Yin, J. Zhang, C. Wang, *Solar RRL* **2020**, *4*, 2000499.

[12] a) M. A. Gerkman, R. S. L. Gibson, J. Calbo, Y. Shi, M. J. Fuchter, G. G. D. Han, *J. Am. Chem. Soc.* **2020**, *142*, 8688; b) Z. Zhang, Y. He, Z. Wang, J. Xu, M. Xie, P. Tao, D. Ji, K. Moth-Poulsen, T. Li, *J. Am. Chem. Soc.* **2020**, *142*, 12256.

[13] Y. B. Zheng, J. L. Payton, C.-H. Chung, R. Liu, S. Cheunkar, B. K. Pathem, Y. Yang, L. Jensen, P. S. Weiss, *Nano Lett.* **2011**, *11*, 3447.

[14] a) A. Mokhtar, R. Morinaga, Y. Akaishi, M. Shimoyoshi, S. Kim, S. Kurihara, T. Kida, T. Fukaminato, *ACS Mater. Lett.* **2020**, *2*, 727; b) S. Nigel Corns, S. M. Partington, A. D. Towns, *Color. Technol.* **2009**, *125*, 249; c) Y. Wu, Z. Q. Guo, W. H. Zhu, W. Wan, J. J. Zhang, W. L. Li, X. Li, H. Tian, A. D. Q. Li, *Mater. Horiz.* **2016**, *3*, 124.

[15] a) L. Ventolà, T. Calvet, M. A. Cuevas-Diarte, X. Solans, D. Mondieig, P. Négrier, J. C. van Miltenburg, *Phys. Chem. Chem. Phys.* **2003**, *5*, 947; b) M. Tasumi, T. Shimanouchi, A. Watanabe, R. Goto, *Spectrochim. Acta* **1964**, *20*, 629.

[16] W. Zhang, X. Ji, C. Zeng, K. Chen, Y. Yin, C. Wang, *J. Mater. Chem. C* **2017**, *5*, 8169.